Journal of Molecular Structure 1145 (2017) 309–320

Contents lists available at ScienceDirect

Journal of Molecular Structure

journal homepage: http://www.elsevier.com/locate/molstruc

Molecular structures and biological activities of (N)-*n*-alkylammonium 2-chloro-3-oxido-1,4-naphthoquinone salts

Dinkar Choudhari [a], Dipali N. Lande [a], Aditi Bagade [a], Shridhar P. Gejji [a], Debamitra Chakravarty [b], Kisan M. Kodam [a], Sunita Salunke-Gawali [a, *]

[a] Department of Chemistry, Savitribai Phule Pune University, Pune 411007, India
[b] Central Instrumentation Facility, Department of Chemistry, Savitribai Phule Pune University, Pune 411007, India

ARTICLE INFO

Article history:
Received 10 April 2017
Received in revised form
16 May 2017
Accepted 17 May 2017
Available online 20 May 2017

Keywords:
Lawsone
Hydrogen bonding
n-alkylamine
Antiproliferative activity
Hydroxynaphthoquinone

ABSTRACT

Single crystal X-ray structures and vibrational spectra of (N)-*n*-alkylammonium 2-chloro-3-oxido-1,4-naphthoquinone salts (alkyl = methyl to octyl, CS-1 to CS-8) possessing X-H···Y (X = N, C and Y=O, Cl) hydrogen bonding and diverse noncovalent interactions have been characterized. Except for the CS-2 and CS-7 rest of the compounds facilitate π···π and Cl···π interactions. The compound CS-3 showed the presence of Cl···O interactions. Electronic structure and spectral characteristics of obtained are in consonance with the density functional theory. These complexes showed remarkable antiproliferative and antifungal activities.

1. Introduction

Biologically active quinones representing naturally occurring secondary metabolites and are found in a variety of plants, fungi, bacterial and insect families attracted significant attention in the literature. Amongst these hydroxynaphthoquinones find applications in medicines, pigmentations, cosmetics, agrochemicals and other functional chemicals for quite some time [1]. Naphthoquinones exhibit wide range biological activities viz., antibacterial, fungicidal, antiinflammatory, antiviral, antiparasitic, antitrypanosome, antiplasmodial agent, antiproliferative, anticancer and antimalarial [2–7]. The toxicological and pharmacological effects of hydroxy naphthoquinone displaying strong dependence on the chemical structure in particular, the number and positions of hydroxy groups, significantly influence the chemical, physical, redox or biological properties. Hydroxynaphthoquinones for example, lawsone, phthiocol, plumbagin, laphachol, juglone are naturally occurring and possess wide range of pharmacological applications (Fig. 1). Lawsone (2-hydroxy-1,4-naphthoquinone) is a natural colorant obtained from heena leaves and widely used in cosmetic industry and explored in pharmacological applications [8]. Phthiocol (2-hydroxy-3-methyl-1,4-naphthoquinone) is synthesized by tubercular bacteria in human intestine [9]. Lapachol (2-hydroxy-3-(2-methyl-1-propenyl)-1,4-naphthoquinone) extracted from lapacho tree and shows cytotoxic activity against several human cancers, among other biological properties [10]. Plumbagin (5-hydroxy-2-methyl-1,4-naphthoquinone) is also known as Chinese medicine and it is isolated from plants of the plumbago family, that shows a wide range of pharmacological activities, including anticancer, antimicrobial, etc [11]. Juglone (5-hydroxy-1,4-naphthoquinone) is a dye commonly used in food and cosmetic industry, with herbicidal properties [12]. 2-chloro-3-hydroxy-1,4-naphthoquinone is a synthetic derivative of lawsone, its successful synthesis [13] dates back to 1924. Hydroxynaphthoquinones are sparingly soluble in water; their solubility can be increased by salt formation. Deprotonation of hydroxyl group occurs in basic medium and the anionic forms generated trigger keto-enol tautomerism in solutions which renders biological activity [14,15] to these systems. In the present endeavor X-ray single crystal structures of (N)-*n*-alkylammonium 2-chloro-3-oxido-1,4-naphthoquinone salts were elucidated following their successful syntheses by *n*-alkyl amines (CS-1 to CS-8 displayed in Fig. 2). The structures were further derived using the density functional theoretic calculations. The earlier investigations

* Corresponding author.
E-mail address: sunitas@chem.unipune.ac.in (S. Salunke-Gawali).

http://dx.doi.org/10.1016/j.molstruc.2017.05.083
0022-2860/

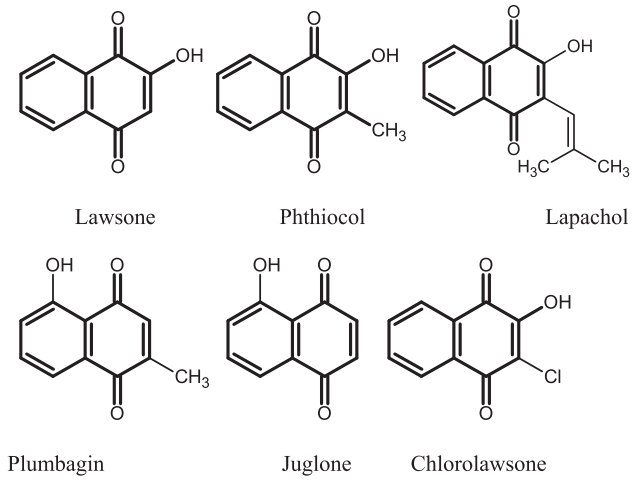

Fig. 1. Naturally occurring hydroxynaphthoquinones.

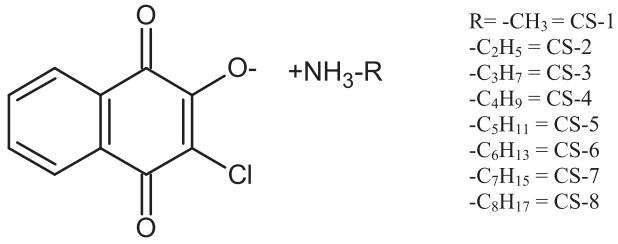

Fig. 2. Molecular structures of CS-1 to CS-8.

on *n*-alkylamino derivatives of 1,4-naphthoquinones have demonstrated that these derivatives possess distinct molecular interactions and biological properties [16–19]. The present investigations focus on how varying alkyl chain of (N)-*n*-alkylammonium cations in chlorolawsonote anion brings forth the distinct molecular interactions which influence their antifungal and anticancer activities. Antifungal activity of CS-1 to CS-6 was evaluated against *Saccharomyces cerevisiae* and *Candida albicans*. Antiproliferative activity was evaluated against breast cancer cell line (MDA-MB-231) and lung cancer cell line (L-132, HeLa derivative).

2. Experimental section

2.1. Materials and methods

2,3-dichloro-1,4-naphthoquinone, ethyl amine solution (70%), propylamine (99%), butylamine (99%), pentylamine (99%), hexylamine (99%), heptylamine (99%) and octylamine (99%) were purchased from Sigma-Aldrich, Methyl amine solution (40%) from Loba chemicals, KOH pellets obtained from Merck Chemicals. Analytical grade dichloromethane, methanol, pet ether, ethyl acetate solvents were purchased from Merck Chemicals. The solvents were distilled by standard methods [20] and dried wherever necessary. FT-IR spectra were recorded between 4000 and 400 cm^{-1} as KBr pellets on the Shimadzu FT 8400 Spectrophotometer. Melting points of compounds were determined using (Make- METLER). ^{1}H (400 MHz) and ^{13}C (100 MHz) NMR of compounds are recorded in DMSO-d_6, on Varian 400 MHz NMR instrument using the TMS (tetramethylsilane) as the reference. UV–Visible spectra of all compounds in methanol were recorded from 200 nm to 800 nm on Shimadzu UV 1800 Spectrophotometer. Elemental analysis was carried out with the Thermo Finnigan EA 1112 Flash series. Elemental Analyzer and on Elementar Vario EL III. The HR-MS spectra were recorded on Bruker impact HD with the ESI source. Gas chromatograph mass spectrums (GC-MS) were recorded on Shimadzu, GC-MS-QP5050.

2.2. Synthesis of 2-chloro-3-hydroxy-1,4-naphthoquinone:chlorolawsone

Modified procedure [21] has been used for synthesis of chlorolawsone. Recrystallized 2,3-dichloro-1,4-naphthoquinone (0.5 g, 2.2 mmol) have been added in 10 ml of water. To this suspension, 10 ml aqueous solution of KOH (0.247 g, 4.4 mmol) was added with constant magnetic stirring. This reaction mixture was heated for 3 hrs at 70 °C. Red color solution was obtained. Unreacted dichlone was extracted with dichloromethane from aqueous reaction mixture and was acidified by adding a few drops of concentrated hydrochloric acid till pH of the reaction mixture becomes pH = 2. Yellow color residue obtained was filtered and washed with diethyl ether and dried over vacuum and subsequently purified by column chromatography and eluted with the ethyl acetate/pet-ether (1:9).

2.3. Synthesis of salts of 2-chloro-3-oxido-1,4-naphthoquninone (N)-n-alkylammonium salts: CS-1 to CS-8

Recrystallization of 2-chloro-3-hydroxy-1,4-naphthoquinone (0.5 g, 2.2 mmol) was carried out by dissolving with 15 ml of dichloromethane (Scheme 1). The mixture was stirred for about 15 min. To this solution, corresponding amines (0.1 ml methyl (CS-1)), (0.29 ml ethyl (CS-2)), (0.485 ml propyl (CS-3)), (0.475 butyl (CS-4)), (0.40 ml pentyl (CS-5)), (0.412 hexyl (CS-6)), (0.428 heptyl (CS-7)), (0.476 octyl amine (CS-8)) solutions were added by drop wise. The reaction mixture was stirred for 24 h at the room temperature (26 °C) with constant magnetic stirring till completion of the reaction that is monitored on TLC. Red colored precipitate thus obtained was filtered and washed with dichloromethane followed by diethyl ether and the residue was dried in vacuum. Subsequently X-ray quality crystals for all these compounds were obtained after recrystallization of solid products in the methanol.

2.3.1. Analytical data of 2-chloro-3-hydroxy-1,4-naphthoquinone: cholorolawsone

Yellow solid, Yield: 0.4 g (87.14%). FT-IR (KBr, cm^{-1}): 3269, 1668, 1639, 1585, 1454, 1363, 1330, 1298, 1273, 1219, 1128, 1008, 856, 727, 682, 599, 538. ^{1}H NMR (400 MHz, DMSO-d_6, δ(ppm)): 8.04 (d, J = 7.5 Hz, 1H), 8.02 (d, J = 7.84 Hz, 1H), 7.86 (td, J = 7.3, 1.3 Hz, 1H), 7.8 (m, 1H).^{13}C NMR (100 MHz DMSO-d_6 (ppm)): 180, 178, 158, 135, 133, 132, 130, 126, 126, 126. UV–Vis: (methanol, λ_{max}, nm): 287, 321, 473. GC-MS (m/z): calcd. for $C_{11}H_{10}ClNO_3$: 208.60; Found: 208.

2.3.2. Analytical data of methyl ammonium-3-chlorolawsonate: CS-1

Red solid, Yield: 0.55 g. (79.82%). Anal. data calcd. for $C_{11}H_{10}ClNO_3$: C, 55.13; H, 4.21; N, 5.84. Found: C, 55.39; H, 4.57; N, 5.90. FT-IR (KBr, cm^{-1}): 3022, 2991, 2980, 1676, 1621, 1516, 1377, 1269, 1155, 1001, 837, 736, 555. ^{1}H NMR (400 MHz, DMSO-d_6, δ (ppm)): 7.91 (d, J = 7.6 Hz, 1H), 7.80 (d, J = 7.5 Hz, 1H), 7.73 (s, 3H), 7.69 (m, 1H), 7.56 (t, J = 7.5 Hz, 1H), 2.42 (s, 3H).^{13}C NMR (100 MHz, DMSO-d_6, δ (ppm)): 25, 113, 125, 125, 130, 131, 134, 135, 167, 174, 184. UV–Vis: (methanol, λ_{max}, nm): 468.

2.3.3. Analytical data of ethyl ammonium-3-chlorolawsonate: CS-2

Red solid, Yield: 0.51 g (83.46). Anal. data calcd. for $C_{12}H_{12}ClNO_3$: C, 56.81; H, 4.77; N, 5.52 Found: C, 56.63; H, 4.52; N, 5.52. FT-IR (KBr, cm^{-1}): 3045, 3010, 2982, 1681, 1579, 1527, 1500,

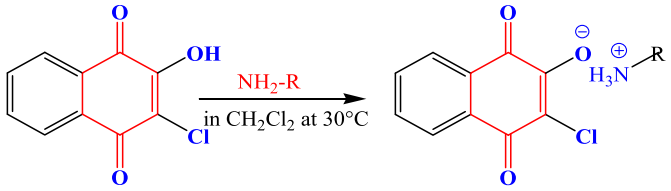

R = -CH_3; CS-1, -C_2H_5; CS-2, -C_3H_7; CS-3, -C_4H_9;CS-4, -C_5H_{11}; CS-5, -C_6H_{13}; CS-6, -C_7H_{15}, CS-7, -C_8H_{19}; CS-8.

Scheme 1. Synthesis of (N)-*n*-alkylammonium 2-chloro-3-oxido-1,4-naphthoquinone.

1317, 1269, 1153, 829, 729, 553. ^{1}H NMR (400 MHz, DMSO-d_6, δ (ppm)): 7.91 (d, J = 7.6 Hz, 1H), 7.79 (d, J = 7.6 Hz, 1H), 7.76 (s, 3H), 7.68 (td, J = 7.5, 1.3 Hz, 1H), 7.55 (td, J = 7.5, 1.2 Hz, 1H), 2.86 (q, J = 7.3 Hz, 2H), 1.16 (t, J = 7.3 Hz, 3H). ^{13}C NMR (100 MHz, DMSO-d_6, δ (ppm)): 184, 174, 167, 135, 134, 131, 131, 125, 125, 113, 34, 13. UV–Vis: (methanol, λ_{max}, nm): 470. HRMS (m/z): calcd. for $C_{12}H_{12}ClNO_3$ $[M+H]^+$: 253.68, found: 254.0575.

2.3.4. Analytical data of propyl ammonium-3-chlorolawsonate: CS-3

Red solid. Yield: 0.556 g (86.33%). Anal. data calcd. for $C_{13}H_{14}ClNO_3$: C, 58.32; H, 5.27; N, 5.23. Found: C, 58.51; H, 5.24; N, 5.35%. FT-IR (KBr, cm^{-1}): 3043, 2987, 2962, 1681, 1589, 1521, 1315, 1269, 1155, 999, 835, 727, 637, 555. ^{1}H NMR (400 MHz, DMSO-d_6, δ(ppm)): 7.90 (d, J = 7.6 Hz, 1H), 7.76 (d, J = 7.6 Hz, 1H), 7.68 (t, J = 7.3 Hz, 1H), 7.55 (t, J = 7.2 Hz, 1H), 7.76 (S, 3H), 2.78 (t, J = 7.5 Hz, 2H), 1.57 (m, 2H), 0.91 (t, J = 7.4 Hz, 3H). ^{13}C NMR (100 MHz, DMSO-d_6, δ (ppm)): 184, 176, 167, 135, 134, 131, 130, 126, 125, 113, 41, 20, 11. UV–Vis; (methanol, λ_{max}, nm): 468. HRMS (m/z): calcd. for $C_{13}H_{14}ClNO_3$ $[M+H]^+$: 267.71, Found: 268.93.

2.3.5. Analytical data of butyl ammonium-3-chlorolawsonate: CS-4

Red solid, Yield: 0.570 g (84.07%). Anal. data calcd. for $C_{14}H_{16}ClNO_3$: C, 59.68; H, 5.72, N, 4.97. Found: C, 60.13; H, 6.00, N: 5.01%. FT-IR (KBr, cm^{-1}): 3136, 3064, 3014, 1678, 1621, 1585, 1523, 1516, 1269, 1220, 1153, 921, 827, 736, 559. ^{1}H NMR (400 MHz, DMSO-d_6, δ (ppm)): 7.90 (d, J = 7.79 Hz, 1H), 7.81 (s, 3H), 7.79 (d, J = 7.8 Hz, 1H), 7.68 (t, J = 7.6 Hz, 1H), 7.55 (d, J = 7.5 Hz, 1H), 2.81 (m, 2H), 1.55 (m, 2H), 1.33 (m, 2H), 0.88 (t, J = 7.3, Hz, 3H). ^{13}C NMR (100 MHz, DMSO-d_6, δ (ppm)): 184, 173, 167, 135, 134, 131, 130, 125, 126, 113, 40, 29, 19, 13: UV–Vis: (methanol, λ_{max}, nm): 468. HRMS (m/z): calcd. for $C_{14}H_{16}ClNO_3$ $[M+H]^+$: 281.08, found: 282.08.

2.3.6. Analytical data of pentyl ammonium-3-chlorolawsonate: CS-5

Red solid, Yield: 0.4 g (86.37%). Anal. data calcd. for $C_{15}H_{18}ClNO_3$: C, 60.91; H, 6.13; N, 4.74, Found: C, 61.02; H, 6.58; N, 4.76. FT-IR (KBr, cm^{-1}): 3144, 3036, 2955, 1680, 1516, 1471, 1375, 1267, 1220, 1039, 999, 829, 732, 673, 557. ^{1}H NMR (400 MHz, DMSO-d_6, δ (ppm)): 7.90 (d, J = 7.6 Hz, 1H), 7.79 (d, J = 7.5 Hz, 1H), 7.72 (s, 3H), 7.67 (m, 1H), 7.54 (m, 1H), 2.51 (m, 2H), 1.53 (m, J = 7.9 Hz, 2H), 1.29 (m, J = 7.9, 4H), 0.87 (t, J = 6.7 Hz, 3H). ^{13}C NMR (100 MHz, DMSO-d_6, δ (ppm)): 184, 174, 167, 135, 134, 131, 131, 125, 125, 113, 39, 28, 27, 22, 14. UV–Vis: (methanol, λ_{max}, nm): 468.

2.3.7. Analytical data of hexyl ammonium-3-chlorolawsonate: CS-6

Red solid, Yield: 0.521 g (87.71%). Anal. data calcd. for $C_{16}H_{20}ClNO_3$: C, 62.03; H, 6.51; N, 4.52. Found: C, 62.28; H, 6.34; N, 4.64. FT-IR (KBr, cm^{-1}): 3136, 3059, 3049, 1678, 1608, 1587, 1525, 1317, 1269, 1155, 989, 829, 736, 559. ^{1}H NMR (DMSO-d_6, 400 MHz, δ (ppm)): 7.92 (d, J = 7.6 Hz, 1H), 7.91 (s, 3H), 7.81 (d, J = 7.6 Hz, 1H), 7.69 (t, J = 7.5 1H), 7.56 (t, J = 7.5, Hz, 1H), 1.54 (t, 2H), 1.27 (m, 7H), 0.84 (t, 3H). ^{13}C NMR (100 MHz DMSO-d_6, δ (ppm)): 184, 173, 167, 135, 134, 131, 131, 125, 125, 113, 39, 31, 27, 25, 22, 14. UV–Vis: (methanol, λ_{max} nm): 468.

2.3.8. Analytical data of heptyl ammonium-3-chlorolawsonate: CS-7

Red solid, Yield: 0.41 g (87.58%). Anal. data calcd. for $C_{17}H_{20}ClNO_3$: C, 63.06; H, 6.85; N, 4.33. Found: C, 63.48; H, 6.73; N, 4.39%. FTIR (KBr, cm^{-1}): 2956, 2981, 2906, 1676, 1585, 1514, 1504, 1269, 1222, 1145, 837, 555. ^{1}H NMR (DMSO-d_6, 400 MHz, δ (ppm)): 7.90 (d, J = 7.2 Hz, 1H), 7.79 (d, J = 7.5 Hz, 1H), 7.73 (s, 3H), 7.76 (t, J = 7.5 Hz, 2H), 2.83–2.74 (m, 2H), 1.52 (m, J = 7.6 Hz), 1.22 (m, J = 7.6 9H), 0.86 (t, J = 6.7 Hz, 3H). ^{13}C NMR (100 MHz, DMSO-d_6, δ (ppm)): 184, 174, 167, 135, 134, 131, 130, 126, 125, 113, 39, 31, 28, 27, 26, 22, 14: UV–Vis: (methanol, λ_{max}, nm): 466.

2.3.9. Analytical data of octyl ammonium-3-chlorolawsonate: CS-8

Red solid, Yield: 0.45 g (93.75%). Anal. data calcd. for $C_{18}H_{24}ClNO_3$: C, 63.99; H, 7.16; N, 4.15. Found: C, 64.35; H, 7.45; N, 4.36. FT-IR (KBr, cm^{-1}): 3138, 3064, 3049, 1678, 1610, 1585, 1516, 1373, 1267, 1219, 1153, 997, 829, 734, 559. ^{1}H NMR (400 MHz, DMSO-d_6, δ (ppm)): 7.91 (d, J = 7.3 Hz, 1H), 7.90 (s, 3 H), 7.80 (d, J = 7.4 Hz, 1H), 7.69 (t, J = 7.4 Hz, 1H), 7.56 (t, J = 7.4 Hz, 1H), 2.81 (m, 2H), 1.54 (m, 2H), 1.25 (m, 10H), 0.81 (d, J = 3H). ^{13}C NMR (100 MHz, DMSO-d_6, δ (ppm)): 184, 174, 167, 135, 134, 131, 130, 126, 125, 113, 38, 31, 28, 27, 26, 22, 14. UV–Vis: (methanol, λ_{max}, nm): 468.

2.4. X-ray crystallographic data collection and refinement of the structures

X-ray quality red crystals of CS-1 to CS-8 were obtained after evaporation of methanol solvent of the respective salt. Data for all the compounds has been collected on D8 Venture PHOTON 100 CMOS diffractometer using graphite monochromatized Mo-K_α radiation (λ = 0.7107 Å) with exposure/frame = 10 s. The X-ray generator was operated at 50 kV and 30 mA. An initial set of cell constants and an orientation matrix were calculated from total of 24 frames. The optimized strategy used for data collection consisted of different sets of φ and ω scans with 0.5° steps in φ/ω. Crystal to detector distance was 5.00 cm with 512 × 512 pixels/frame, Oscillation/frame −0.5°, maximum detector swing angle = −30.0°, beam centre = (260.2, 252.5), in plane spot width = 1.24. Data integration was carried out by Bruker SAINT Program and empirical absorption correction for intensity data were carried out by Bruker SADABS. The programs are integrated in APEX II package [22]. The data were corrected for Lorentz and polarization effect. The structure was solved by Direct Method using SHELX-97 [23]. The final refinement of the structure was carried out by full-matrix least-squares techniques with anisotropic thermal data for non-hydrogen atoms on F^2. The non-hydrogen atoms were

refined anisotropically, whereas the hydrogen atoms were refined at the calculated positions as riding atoms with isotropic displacement parameters. Molecular diagrams were generated using ORTEP-3 [24] and Mercury programs [25]. Structural calculations were performed using the SHELXTL [23] and PLATON [26].

2.5. Density functional theory

Geometry optimizations of naphthoquinone derivatives were carried out within the framework of Density Functional Theory (DFT) with the use of Gaussian 09 suite of programs [27]. The hybrid M06-2X exchange correlation functional in conjunction with 6-311 + G(d,p) basis set was employed. Net atomic charges are derived from natural bond order analysis. Stationary point structures thus derived were confirmed to be the local minima on the potential energy surfaces through the vibrational frequency calculations. All the normal vibrational frequencies of these stationary point structures turned out to be real. The normal vibrations were assigned by visualizing the atomic displacements around their equilibrium (mean) positions with the help of GAUSSVIEW-5 program [28]. Frontier orbitals were computed within the same framework of theory.

2.6. Antimicrobial activity

The antifungal activity was studied against *Saccharomyces cerevisiae* NCIM 3559 and *Candida albicans* ATCC 10231. Compounds were dissolved in DMSO with a stock concentration of 20 mg/ml which were further serially diluted in sterile distilled water. Reaction volume was maintained at 100 μl in sterile 96 well plates. Each well consisted of varying concentration of test compound, 67.5 μg of resazurin (BDH) along with fungal cultures were added. Volume was made up to 100 μl with 3.3× autoclaved Sabouraud's medium (Hi-Media, India). A column of wells with all solutions except fungal cultures was taken a negative control. All the solutions except the test compound were also taken as a negative control. DMSO control consisted of different concentrations of DMSO utilized without addition of the test compounds to examine toxicity by DMSO. Commercially available antibiotic, amphotericin B was used as positive control. The 96 well plates were incubated at 37 °C for 48 h. All the experiments were carried out in triplicate. Color change from blue to pink was assessed visually. The concentration that accompanies the color change was taken as the MIC value [29].

2.7. Antiproliferative activity

The antiproliferative activities were examined using the MTT [3-(4,5-dimethylthiazol-2-yl)-2,5-diphenyltetrazolium bromide] assay on a MDA-MB-231 (breast cancer) and L-132 (lung cancer, HeLa derivative) cell lines. The MTT assay was used to assess the anti-proliferative activity of these compounds. MDA-MB-231 cells were maintained in Leibovit's 15 medium and L-132 cells were maintained in DMEM medium at 37 °C with 5% CO_2. The varying concentrations of (5, 25, 50, 100, and 200 μg/ml) compounds were incubated with 2×10^5 cells/ml of MDA-MB-231 cell line for 48 h and L-132 cell line for 24 h in CO_2 incubator (Nuaire, USA). After incubation, culture media was removed from the 96 well culture plates and cells were washed with phosphate buffered saline till the color of compounds was removed, 40 μg of MTT was added per well and incubated for 3 h in CO_2 incubator. After incubation, the formazan crystals formed in wells were solubilized in 100 μl of DMSO and kept for 5–10 min for complete dissolution of formazan and then absorbance was measured at 580 nm on multimode plate reader (Multimode plate reader, Enspire, Perkin Elmer) [30].

3. Results and discussion

3.1. FT-IR, ^1H and ^1C NMR UV–Visible studies

FT-IR spectra of CS-1 to CS-8 revealed a broad band between 3250 and 2500 cm^{-1} (Fig. S1 in ESI†) that arises from the overlapped bands of the –NH as well as –CH stretching's. The carbonyl frequency was increased by18 cm^{-1} while *p*-naphthoquinone frequency was decreased by ~20 cm^{-1} when compared with free chlorolawsone (Table 1). ^1H and ^{13}C chemical shifts are assigned from the ^1H and ^{13}C and DEPT experiments (Fig. S2-S10, Tables S2 and S3 in ESI†). The proton chemical shifts of the ammonium cation were observed in ~ δ = 7.73–7.91 ppm region (Table S2 in ESI†). As may also be observed the ^{13}C chemical shifts (in ppm) follows the order: C(2) (113) < C(3) (167) < C(4) (174) < C(1) (184 ppm) as displayed in Table S3 (in ESI†) of the supporting information. Thus C(3), C(4) reveal significant deshielded signals compared to the free chlorolawsone. The UV–visible spectra for CS-1 to CS-8 along with the chlorolawsone were recorded with 4×10^{-4} M concentration in methanol (Fig. S11). The peak centered at ~468 nm in UV–visible spectra of all compounds was assigned using time dependent DFT computations.

3.2. Single crystal X-ray diffraction studies

ORTEP plots of CS-1 to CS-8 are portrayed in Fig. 3. The crystal structure data is summarized in Table 2. Moreover, the hydrogen bonding parameters are given in Table S34 (in ESI†). As may readily be noticed CS-1 crystallizes in triclinic space group *P-1* while CS-4 and CS-8 in *P1*. CS-2, CS-3, CS-5 and CS-7 crystallize in monoclinic space group $P2_1/c$ and CS-6 reveals the $P2_1$ space group. The bond distances C(1)–O(1), C(3)–O(2), and C(4)–O(3) respectively, are observed to be ~1.24 Å, ~1.26 Å and ~1.211 Å [14,31–35]. As revealed further from the X-ray data the carbonyl bond distances are closer to those observed in the anionic form of hydroxynaphthoquinone [35]. A delocalization of electron density on the quinonoid moiety hence, can be inferred.

Table 1
Prominent stretches in salts CS-1 to CS-8 from DFT studies, the experimental values are given in parenthesis.

Compounds	ν_{OH}	ν_{NH}	ν_{NH+} ν_{CH}	$\nu_{4(C1=O1)}$	$\nu_{4(C4=O2)}$	$\nu_{1(C=C)}$
Chlorolawsone	3456(3272)		–	1696(1659)	1676	(1582)
CS-1	–	3364	2422(3015)	1678(1678)	1670	1584(1582)
CS-2	–	3362	2369(2979)	1678(1678)	1671	1583(1582)
CS-3	–	3353	2384(2961)	1675(1678)	1666	1588(1588)
CS-4	–	3362	2369(2955)	1676(1678)	1672	1587(1580)
CS-5	–	3347	2410(2944)	1677(1678)	1669	1582(1588)
CS-6	–	3366	2371(2955)	1685(1678)	1679	1590(1594)
CS-7	–	3351	2460(2920)	1681(1678)	1672	1579(1582)
CS-8		3351	2351(2913)	1677(1678)	1672	1587(1594)

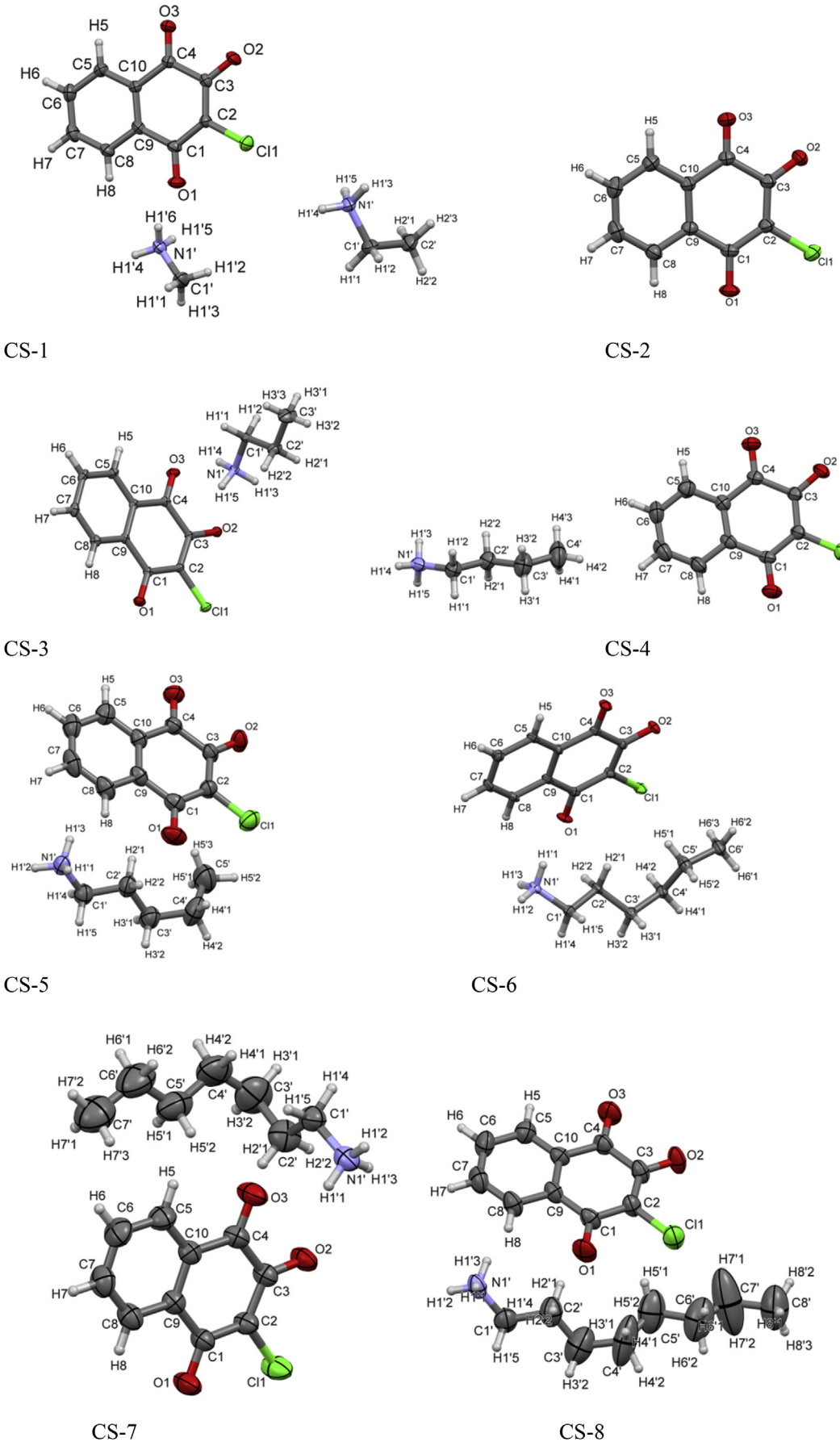

Fig. 3. ORTEP plots of CS-1 to CS-8. The ellipsoids were drawn with 50% probability.

Table 2
Crystallography parameter of CS-1 to CS-8.

Identification code	CS-1	CS-2	CS-3	CS-4
CCDC	1,504,336	1,504,330	1,504,334	1,504,329
Empirical formula	$C_{11}H_{10}ClNO_3$	$C_{12}H_{12}ClNO_3$	$C_{13}H_{14}ClNO_3$	$C_{14}H_{16}ClNO_3$
Formula weight	239.65	253.68	267.70	281.73
Temperature	296(2) K	200(2) K	100(2) K	296(2) K
Wavelength	0.71073 Å	1.54178 Å	1.54178 Å	0.71073 Å
Crystal system	Triclinic	Monoclinic	Monoclinic	Triclinic
Space group	*P -1*	*P 2₁/c*	*P 2₁/c*	*P 1*
Unit cell Dimensions	a = 7.382(8) Å, b = 8.611(8) Å, c = 9.270(8) Å α = 98.46(5)°, β = 109.34(4)°, γ = 106.58(5)°	a = 13.2023(5) Å a = 90°. b = 10.6791(5) Å b = 102.524(2)°. c = 8.1788(4) Å β = 102.524(2)°	a = 7.2690(4)Å, b = 15.4708(8)Å c = 11.5339(6)Å β = 97.628(2)°,	a = 5.0099(5)Å, b = 8.2750(8)Å, c = 9.1878(10)Å α = 112.829(3)°, β = 96.095(3)°, γ = 90.889(3) °.
Volume	513.5(8) $Å^3$	1125.68(9) $Å^3$	1285.59(12) $Å^3$	348.41(6) $Å^3$
Z	2	4	4	1
Density (calculated)	1.550 Mg/m^3	1.497 Mg/m^3	1.383 Mg/m^3	1.343 Mg/m^3
Absorption coefficient	0.361 mm^{-1}	2.989 mm^{-1}	2.646 mm^{-1}	0.277 mm^{-1}
F(000)	248	528	560	148
Crystal size	0.139 × 0.109 × 0.093 mm^3	0.231 × 0.137 × 0.071 mm^3	0.42 × 0.19 × 0.06 mm^3	0.28 × 013 × 0.07 mm^3
Theta range for data collection	3.113–24.986°.	5.379–68.288°.	4.810–68.307°.	2.676–28.420°.
Index ranges	−8 ≤ h<=8, 10 ≤ k<=10, −11 ≤ l<=11	−15 ≤ h<=15, −12 ≤ k<=12, −9 ≤ l<=9	−8 ≤ h<=8, −18 ≤ k<=18, −13 ≤ l<=13	−6 ≤ h<=6, −11 ≤ k<=10, −12 ≤ l<=12
Reflections collected	10950	9708	13393	7388
Independent reflections	1782 [R(int) = 0.0746]	2012 [R(int) = 0.0757]	2338 [R(int) = 0.0421]	3287 [R(int) = 0.0318]
Completeness to θ = 25.242°	96.0%	97.5%	99.0%	99.9%
Refinement method	Full-matrix least-squares on F^2	Full-matrix least-squares on F^2	Full-matrix least-squares on F^2	Full-matrix least-squares on F^2
Data/restraints/parameters	1782/0/147	2012/0/156	2338/0/165	3287/3/174
Goodness-of-fit on F^2	1.067	1.087	1.007	1.059
Final R indices [I > 2 σ(I)]	R1 = 0.0558, w*R2* = 0.1630	R1 = 0.0775, w*R2* = 0.2085	R1 = 0.0324, w*R2* = 0.0833	R1 = 0.0438, w*R2* = 0.0822
R indices (all data)	R1 = 0.0885, w*R2* = 0.2030	R1 = 0.0981, w*R2* = 0.2245	R1 = 0.0358, w*R2* = 0.0864	R1 = 0.0722, w*R2* = 0.0929
Extinction coefficient	n/a	n/a	n/a	n/a
Largest diff. peak and hole	0.432 and −0.614 e.$Å^{-3}$	0.547 and −0.568 e.$Å^{-3}$	0.245 and −0.337 e.$Å^{-3}$	0.188 and −0.224 e.$Å^{-3}$

Identification code	CS-5	CS-6	CS-7	CS-8
	1,504,335	1,504,332	1,504,331	1,504,333
Empirical formula	$C_{15}H_{18}ClNO_3$	$C_{16}H_{20}ClNO_3$	$C_{17}H_{22}ClNO_3$	$C_{18}H_{20}ClNO_3$
Formula weight	295.75	309.78	323.80	333.80
Temperature	200(2) K	296(2) K	296(2) K	296(2) K
Wavelength	1.54178 Å	1.54178 Å	1.54178 Å	1.54178 Å
Crystal system	Monoclinic	Monoclinic	Monoclinic	Triclinic
Space group	*P 2₁/c*	*P 2₁*	*P 2₁/c*	*P 1*
Unit cell dimensions	a = 4.8891(3) Å b = 15.3434(9) Å c = 19.7154(12) Å β = 94.069(3)°	a = 8.0710(4) Å b = 4.8513(3) Å c = 20.3990(10) Å β = 100.119(2)°	a = 10.101(2) Å b = 15.606(3) Å, c = 11.531(2) Å β = 112.871(9)°	a = 5.0846(2) Å, α = 92.780(2)° b = 8.2238(4) Å, β = 90.898(2)° c = 10.5386(5) Å, γ = 90.756(2)°
Volume	1475.23(15) $Å^3$	786.30(7) $Å^3$	1674.8(6) $Å^3$	440.05(3) $Å^3$

Z	4	2	4	1
Density (calculated)	1.332 Mg/m^3	1.308 Mg/m^3	1.284 Mg/m^3	1.260 Mg/m^3
Absorption coefficient	2.355 mm^{-1}	2.232 mm^{-1}	2.118 mm^{-1}	2.035 mm^{-1}
F(000)	624	328	688	176
Crystal size	0.23 × 0.14 × 0.07 mm^3	0.482 × 0.216 × 0.113 mm^3	0.22 × 0.20 × 0.04 mm^3	0.31 × 0.15 × 0.09 mm^3
Theta range for data collection	4.497–68.167°.	5.568–68.405°	4.751–68.661°.	4.200–68.504°.
Index ranges	$-5 \le h \le 5, -18 \le k \le 18, -23 \le l \le 23$	$-9 \le h \le 9, -5 \le k \le 5, -24 \le l \le 24$	$-12 \le h \le 12, -18 \le k \le 18, -13 \le l \le 13$	$-6 \le h \le 6, -9 \le k \le 9, -12 \le l \le 12$
Reflections collected	8277	9180	26869	7000
Independent reflections	2624 [R(int) = 0.0612]	2584 [R(int) = 0.0855]	3082 [R(int) = 0.0671]	2774 [R(int) = 0.0392]
Completeness to theta = 67.679°	97.6%	99.3%	100.0%	99.1%
Absorption correction	Semi-empirical from equivalents	Semi-empirical from equivalents	Semi-empirical from equivalents	Semi-empirical from equivalents
Max. and min. transmission	0.848 and 0.707	0.777 and 0.589	0.919 and 0.659	0.833 and 0.728
Refinement method	Full-matrix least-squares on F^2	Full-matrix least-squares on F^2	Full-matrix least-squares on F^2	Full-matrix least-squares on F^2
Data/restraints/parameters	2624/0/183	2584/1/193	3082/0/201	2774/3/210
Goodness-of-fit on F^2	1.018	1.055	1.031	1.064
Final R indices [I > 2sigma(I)]	R1 = 0.0554, wR2 = 0.1295	R1 = 0.0528, wR2 = 0.1358	R1 = 0.0538, wR2 = 0.1161	R1 = 0.0641, wR2 = 0.1760
R indices (all data)	R1 = 0.0807, wR2 = 0.1479	R1 = 0.0598, wR2 = 0.1398	R1 = 0.0974, wR2 = 0.1375	R1 = 0.0663, wR2 = 0.1787
Extinction coefficient	n/a	n/a	n/a	n/a
Largest diff. peak and hole	0.232 and −0.271 $e.Å^{-3}$	0.368 and −0.473 $e.Å^{-3}$	0.181 and −0.227 $e.Å^{-3}$	0.312 and −0.246 $e.Å^{-3}$

Table 3
Molecular interactions in CS-1 to CS-8 (interaction √ = present, × = absent).

Compound	C→A	A→A	N–H···Cl	C–H···O	C–H···Cl	Cl ··· π/π ··· π
CS-1	4	3	✓	✓	✓	π ··· π
CS-2	5	–	×	✓	✓	×
CS-3	3	2	✓	✓	×	π ··· π, Cl···O
CS-4	3	2	✓	✓	×	Cl ··· π, π ··· π
CS-5	4	2	×	✓	×	π ··· π
CS-6	4	2	✓	✓	✓	Cl ··· π
CS-7	3	–	✓	×	✓	×
CS-8	4	2	✓	×	×	Cl ··· π, π ··· π

C = *n*- alkyl ammonium.
A = 3-chloro-2-oxido-1,4-naphthoquinone.

Chlorolawsone anion and *n*-alkyl ammonium cation hydrogen bonding and π-π stacking interactions (Fig. S16 in ESI†) are displayed in Table 3. All compounds reveals strong N–H···O interactions in addition to a variety of N–H···Cl, C–H···O, C–H···Cl interactions. Except for CS-2 and CS-7 the π···π and Cl···π interactions (Table 3) are also noticed. Besides the CS-3 crystal structure shows the presence of Cl···O interactions.

Stair case like polymeric chain of CS-1 molecules is formed via N–H···O and C–H···O interaction (Fig. 4a). As shown in Fig. 4a the crystal structure of CS-1 shows the cation is bound to two anions and vice a versa via hydrogen bonding interactions. Further a dimeric chain observed in the crystal structure further facilitated by N–H···O interactions in addition to C(8)···C(8)(1-x,1-y,1-z, 3.346 Å) stacking. Polymeric chain of CS-2 extends via N–H···O and C–H···O interactions, which further links to nearby polymeric chain via N–H···O and C–H···Cl (1 + x, y, −1+z) interactions displayed in Fig. 4b down the c-axis.

Molecular packing of CS-3 is shown in Fig. 4c down the a-axis. With the reverse orientation of the molecules the benzenoid and quinonoid rings exhibit π···π stacking with their separation being 3.534 Å. Polymeric chain of cation and anion of CS-4 are formed via N–H···O, C–H···O and C–H···Cl interaction as shown in Fig. 4d down the a-axis. Besides Cl···π interactions are observed in CS-4 anions which are evidenced from the C(4)···Cl(1) (3.370(3) Å, −1+x, y, z) and C(5)···C(1) close contacts (3.355(5) Å, −1+x, y, z). Polymeric network of CS-5 is formed via N–H···O and C–H···O interactions, as displayed in Fig. 4e. In addition to these interactions Cl···π interactions between the centroid of quinonoid ring to chlorine (3.519 Å, −1+x, y, z) are observed. Polymeric chain in CS-6 molecules extends by N–H···O, N–H···Cl, C–H···O and C–H···Cl interactions where the neighboring polymeric chains are linked by C(6)–H(6)···O(3) (1-x, +1/2 + y, 1-z) as shown in Fig. 4f. Unlike CS-5, CS-6 also showed Cl···π interaction of chlorine to centroid of the quinonoid ring (3.438 Å, x, −1+y, z). CS-7 is void of π···π stacking or Cl···π interactions. Tetrameric unit of CS-7 comprises of two cations and two anions which is facilitated through N–H···O interaction arising from O(2) and O(3) oxygens those are further linked by N–H···O interactions of O(1) (Fig. 4g). Molecular packing of CS-8 shows polymeric chain comprising of alternate cation and anion formed via the N–H···O interaction along the b-axis wherein the anionic chain reveals Cl···π interactions with the quinonoid ring of the adjacent anion (3.453 Å, 1 + x, y, z). The C(5) and C(1) close contacts also can be inferred as displayed in Fig. 4h.

3.3. DFT investigations

Optimized structures of chlorolawsone and CS-1 to CS-8 are shown in Fig. 5. Atomic labeling scheme as well as net atomic charges are also given along with. An isomer with the hydroxyl placed at C(3) position is turned out to be of the lowest energy.

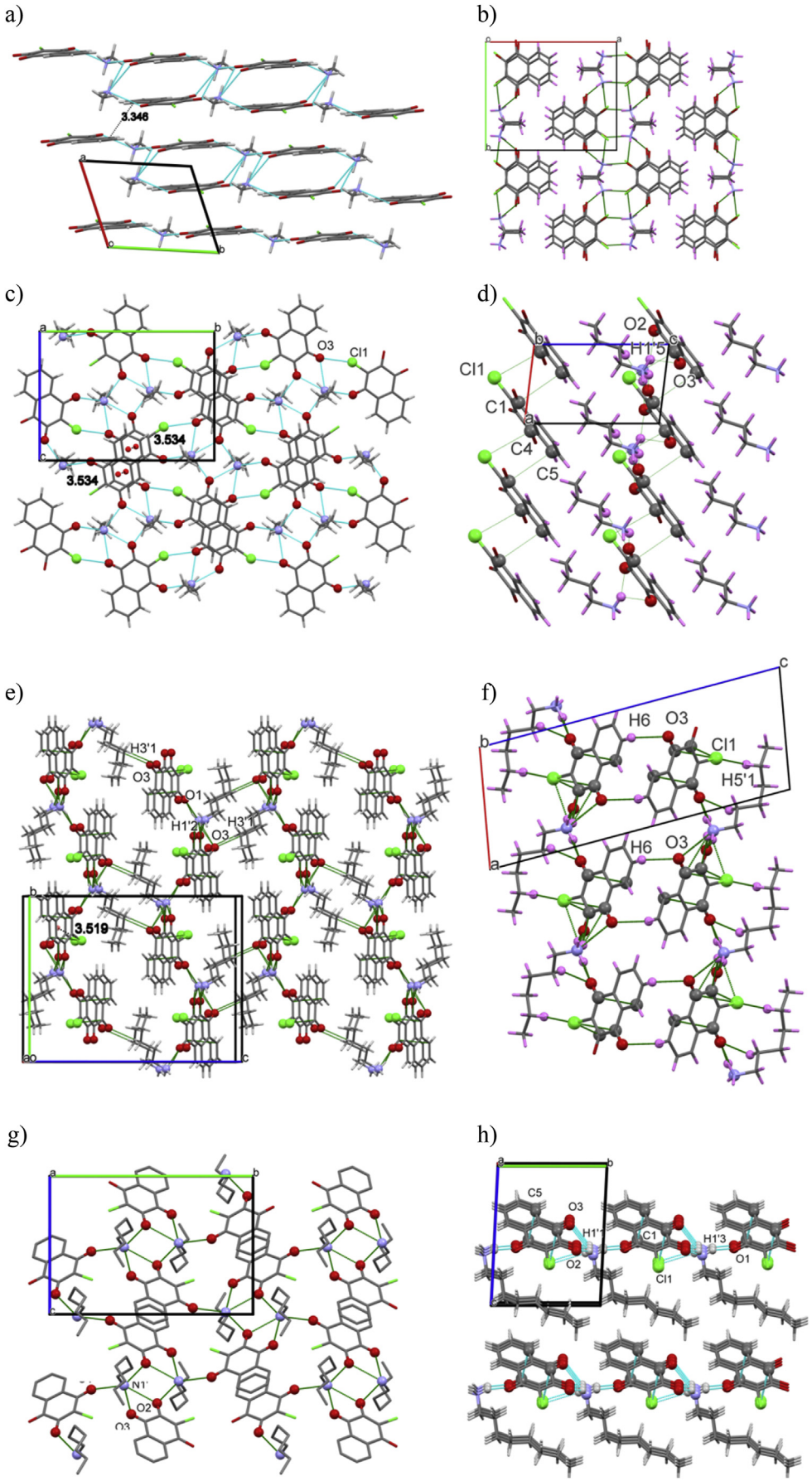

Fig. 4. Molecular packing of a) CS-1 down c axis, b) CS-2 down c axis, c) CS-3 down c-axis, d) CS-4 down b-axis, e) CS-5 molecule, f) Polymeric chain s of CS-6 down b-axis, g) CS-7 down a-axis, h) CS-8.

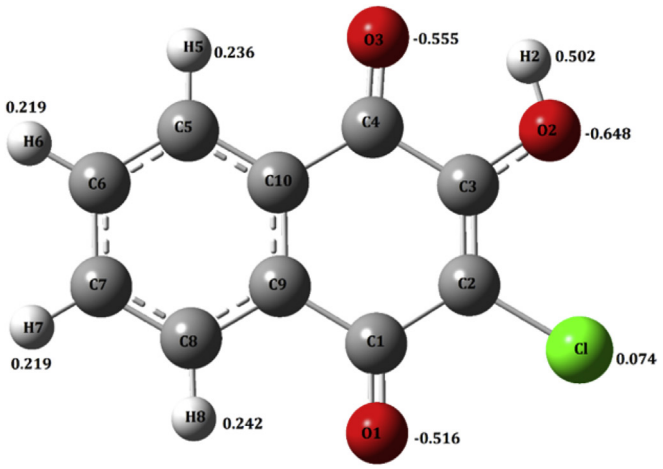

(a) (0.0 kJ mol^{-1})

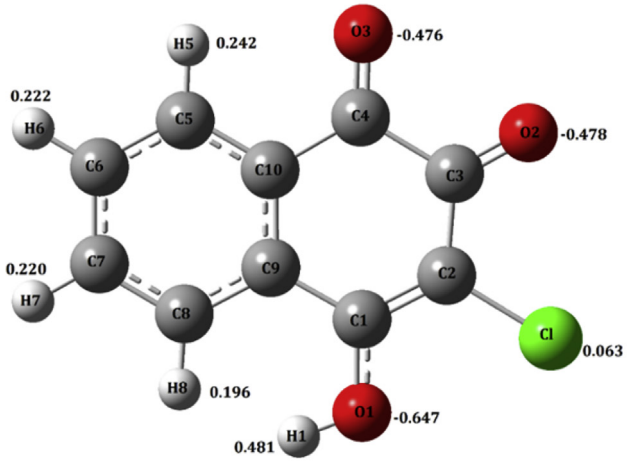

(b) (61.5 kJ mol^{-1})

Fig. 5. Isomers of chlorolawsone (isomer 'a' is more stable).

The charge distribution is characterized by the molecular electrostatic potential (MESP) mapped topography as illustrated in Fig. 6. It is thus evident that effective electron rich regions (red) are located around the domain of lone pair residing on the oxygen atom centers whereas the large electron deficient regions are characterized near the vicinity of hydroxyl functionalities; which is consistent with net atomic charges derived from the NBO analysis. The molecular structures comprising of varying alkyl chain and amide group was obtained which is reported in Fig. 7. The interactions between nitrogen lone pair and the hydroxyl proton may further be inferred. A proton transfer is evident with concomitant increase of O(2)–H(2) bond distance (up to ~0.0656 Å) in all these systems. Interestingly the proton transfer which results in the disappearance of ~3456 cm^{-1} vibration in 2-chloro-3-hydroxy-1,4-naphthoquinone, the parent compound. A new intense band in the range of 2351 cm^{-1}- 2422 cm^{-1} can readily be noticed. Subsequently C(3)–O(2) carbonyl stretching was observed near ~1678 cm^{-1}. Noteworthy enough an increasing

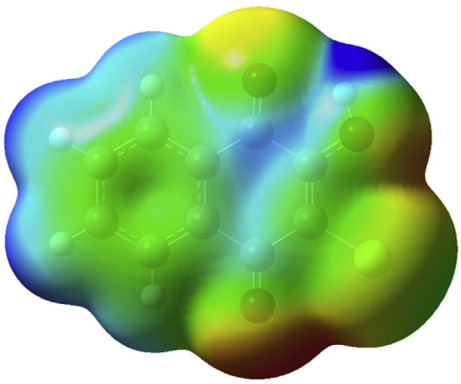

Fig. 6. MESP mapped density of chlorolawsone.

alkyl chain length has no significant effect on characteristic stretching vibrational frequency. Fig. 8 illustrates characterize the charge distribution in the methyl complex. Frontier orbital analysis clearly shows that HOMO and LUMO resides over the naphthoquinonoid moiety. Interestingly the HOMO and LUMO for the rest of molecules are strikingly similar as shown in Fig. S17 (in ESI†) of the supporting information. MESP isosurfaces in these systems are also displayed.

3.4. Antifungal activity

The compounds CS-1 to CS-6 showed inhibition against *S. cerevisiae* than *C. albicans*. Standard antifungal amphotericin B showed MIC of 1.25 mg/ml for both the strains (Table 4). Antifungal activities of CS-3 and CS-4 against *S. cerevisiae* were better than amphotericin B with MIC values being the least for the CS-3. The MIC value decreased from 2.5 mg/ml for CS-1 to 0.009 mg/ml for CS-3 and 0.625 mg/ml for CS-4, further it increased to 2.5 mg/ml for the CS-5. In *C. albicans* the MIC value was 10 mg/ml for CS-1, which is same i.e. 5 mg/ml for the CS-2 to CS-6 compounds.

A variety of controls were used in this study, negative control which did not contain any test compound exhibited pink color. Blue colored indicator dye resazurin was reduced to resofurin which subsequently was reduced to hydroresofurin by oxidoreductases from live cells giving pink color. The control without microbial culture showed blue color since the resazurin was not reduced. DMSO control at all concentrations showed pink color that renders non-toxicity to microbes used.

3.5. Antiproliferative activity

The first four members (carbon 1 to 4) of homologated (N)-*n*-alkylamino1,4-naphthoquinone derivatives showed enhanced biological activity as compared the rest of the members [16–19]. Cohesive interactions are observed in *n*-alkylamines in five or more carbon atoms; the biological activities are thus hindered by such molecular interactions. Hence we studied antiproliferative activity of first four members of (N)-*n*-alkylammonium 2-chloro-3-oxidio-1,4-naphthoquinone salts, CS-1 to CS-4. Compounds CS-1 to CS-4 showed antiproliferative activity against MDA-MB-231 breast cancer cell line. CS-1 showed the minimum IC_{50} of 37.6 ± 3.1 μg/ml, with increasing carbon chain-length the IC_{50} value increases for CS-2 (51.0 ± 13.5 μg/ml) and CS-3 (58.2 ± 10.4 μg/ml). A decrease of 47.6 ± 2.5 μg/ml in the CS-4 was also noticed. On the other hand, antiproliferative activity against lung cancer cell line L-132 (HeLa derivative) showed lower activity than the standard methotrexate.

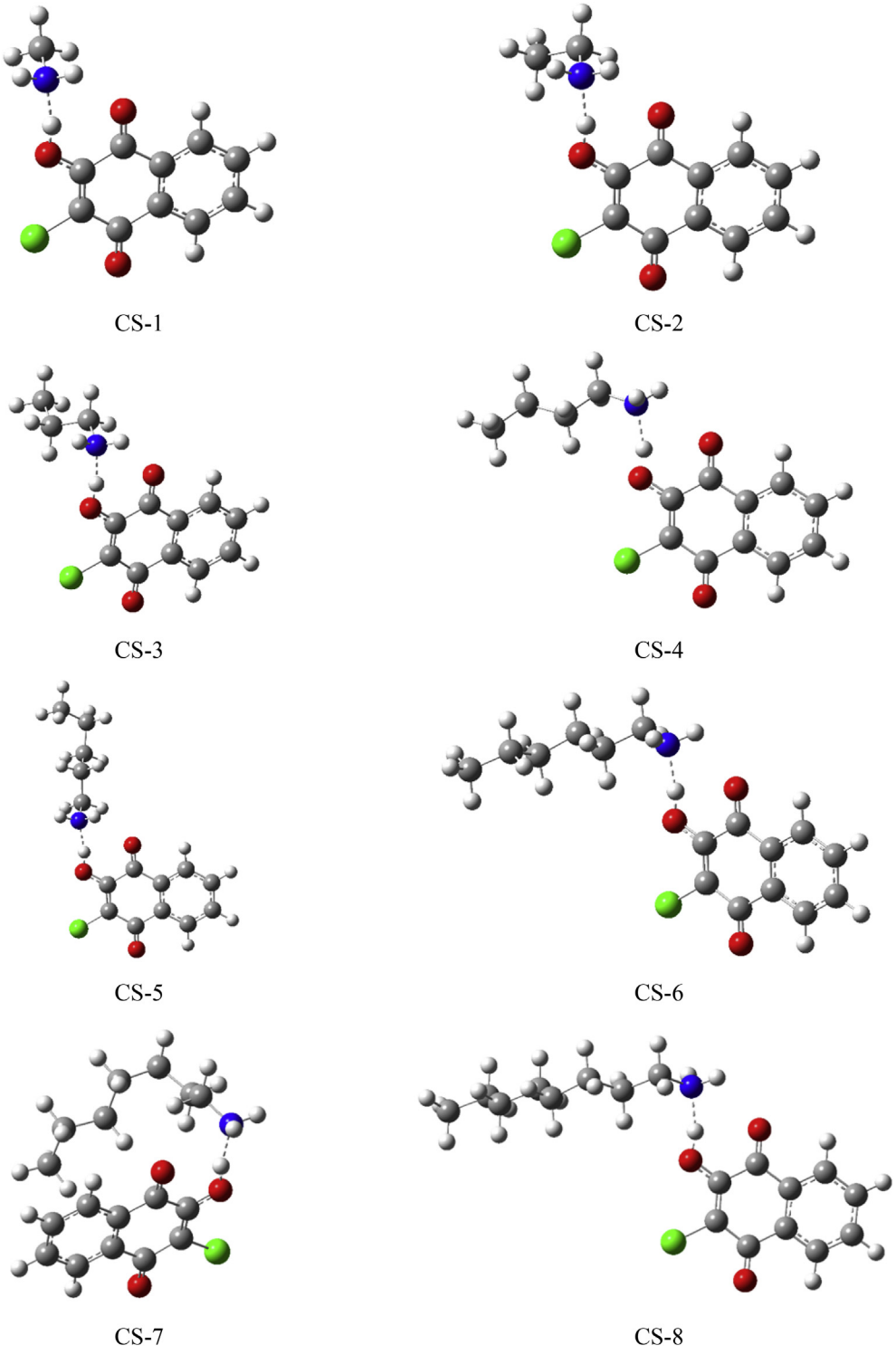

Fig. 7. Optimized geometries of CS-1 to CS-8.

The compounds, CS-2 showed maximum IC_{50} of 150 ± 5.2 μg/mL, CS-1 showed 124 ± 0.54 μg/mL, CS-3 exhibited 105 ± 12.8 μg/mL and CS-4 showed least IC_{50} value of 95 ± 1.24 μg/mL (Table 5). The DMSO control showed negligible antiproliferative activity. The antiproliferative studies further demonstrate that these compounds are more effective on breast cancer MDA-MB-281 cell line than lung cancer L-132 cell line.

4. Conclusions

A family of (N)-*n*-alkylammonium 2-chloro-3-oxido-1,4-naphthoquinone salts have been synthesized and characterized using the single crystal X-ray diffraction in conjunction with the density functional theory. Diverse molecular interactions in CS-1 to CS-8 are analyzed. The antifungal activities points to CS-1 to CS-6

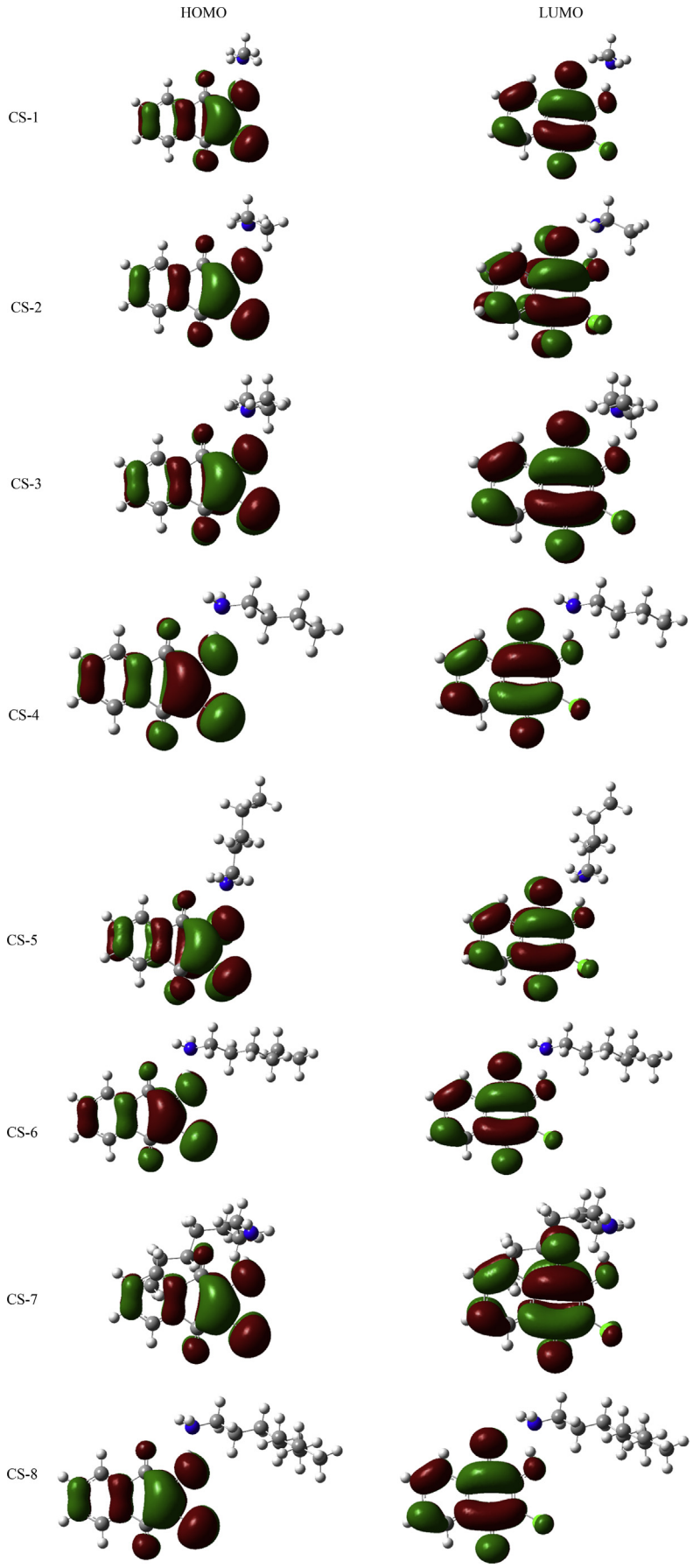

Fig. 8. Frontier orbitals in CS-1 to CS-8.

Table 4
Antifungal activity of CS-1 to CS-6 (MIC values are in mg/ml).

Samples	Minimum inhibitory concentration (MIC) mg/ml	
	Saccharomyces cerevisiae NCIM 3559	*Candida albicans* ATCC 10231
CS-1	2.5	10
CS-2	2.5	5
CS-3	0.009	5
CS-4	0.625	5
CS-5	2.5	5
CS-6	1.25	5
Amphotericin B (Standard)	1.25	1.25

Table 5
Anti-proliferative activity (IC_{50} values) of CS-1 to CS-4 on breast cancer (MDA-MB-231) and lung cancer (L-132, HeLa derivative) cell lines.

Samples	IC_{50} μg/ml	
	Breast cancer cell line (MDA-MB-231)	Lung cancer cell line (L-132)
CS-1	37.6 ± 3.1	124 ± 0.5
CS-2	51.0 ± 13.5	150 ± 5.2
CS-3	58.2 ± 10.4	105 ± 12.8
CS-4	47.6 ± 2.5	95 ± 1.2
Methotrexate (standard)	18.4 ± 3.2	6.2 ± 1.2

are promising against *Saccharomyces cerevisiae* and *Candida albicans*. The antiproliferative activity measurements suggest CS-1 to CS-4 is effective against breast cancer cell line (MDA-MB-231) than lung cancer cell line (L-132). The active components in CS-1 to CS-6 was further shown to be 2-chloro-3-oxido-1,4-naphthoquinone anion whereas the *n*-alkylammonium cation does not influence the biological activities. Cytotoxicity of quinone compounds can be explained because of their redox ability and generation of reactive oxygen species. With the increasing alkyl chain, a decrease of redox potential of naphthoquinone/naphthosemiquinone redox couple can be noticed, which in turn has direct impact on the superoxide radical generation and hence, the cytotoxic activity, however this is not the only mechanism followed by the hitherto compounds and possibly more than one mechanistic pathways led to cytotoxic activity to these compounds. Increasing alkyl chain of the cation as in hitherto compounds restricts their interactions with DNA. Alternatively steric effects may prove crucial in this respect. Besides redox cycling of naphthoquinones, their optimum size and non covalent interacting modes with DNA are key factors, which possibly govern their biological activities.

Acknowledgements

SSG grateful to RGYI scheme of Department of Biotechnology, New Delhi, India for Ref. No. (BT/PR6565/GBD/27/456/2012). DC thankful to UGC for meritorius fellowship. SPG acknowledges support from the Research Project (37(2)/14/11/2015-BRNS) from the Board of Research in Nuclear Sciences (BRNS), India. DNL is thankful to Savitribai Phule Pune University for the award of research fellowship through the University of Potential excellence scheme from the University Grants Commission, New Delhi, India. SPG and DNL thank the Center for Development of Advanced Computing (CDAC), Pune for providing National Param Supercomputing Facility.

Appendix A. Supplementary data

Supplementary data related to this article can be found at http://dx.doi.org/10.1016/j.molstruc.2017.05.083.

References

[1] R.H. Thomson, Naturally Occurring Quinones, Academic Press, New York, 1971.
[2] V.K. Tandon, D.B. Yadav, R.V. Singh, M. Vaish, A.K. Chaturvedi, P.K. Shulka, J. Bio-Org Med. Chem. Lett. 15 (2005) 3463–3466.
[3] A.E. Shchekoikhin, V.N. Buyanov, M.N. Preobrazhenskaya, J. Bio-org. Med. Chem. 12 (2004) 3923–3930.
[4] J.C. Lien, L.J. Huang, J.P. Wang, C.M. Teng, K.H. Lee, S.C. Kuo, Bio-Org. Med. Chem. 5 (1997) 2111–21120.
[5] E.J. Lee, H.J. Lee , H.J. Park, H.Y. Min, M.E. Suh, H.J. Chung, S.K. Lee, Bio-org. Med. Chem. Lett. 14 (2004) 5175–5178.
[6] G.Y. Song, Y. Kim, X.G. Zheng, Y.J. You, H. Cho, J.H. Chung, D.E. Sok, B.Z. Ahn, Eur. J. Med. Chem. 35 (2000) 291–298.
[7] L.S. Chemin, E. Buisine, V. Yardley, S. Kohler, M.A. Debreu, V. Landry, C. Sergheraert, S.L. Croft, R.L.K. Siegel, E.D. Charvet, J. Med. Chem. 44 (2001) 548–565.
[8] R. Pradhan, P. Dandawate, A. Vyas, S. Padhye, B. Biersack, R. Schobert, A. Ahmad, F.F.H. Sarkar, Curr. Drug Targets 13 (2012) 1777–1798.
[9] R.J. Anderson, M.S. Newman, J. Biol. Chem. 103 (1933) 197–201.
[10] H. Hussain, K. Krohn, V.U. Ahmad, G.A. Miana, I.V. Green, ARKIVOC 2 (2007) 145–171.
[11] S. Padhye, P. Dandawate, M. Yusufi, A. Ahmad, F.H. Sarkar, Med. Res. Rev. 32 (2012) 1131–1158.
[12] J-J. Lu, J.-L. Bao, G.-S. Wu, W.-S. Xu, M.-Q. Huang, X.-P. Chen, Y.-T. Wang, Anti-Cancer Agents Med. Chem. 13 (2013) 456–463.
[13] J.B. Conant, L.F. Fieser, J. Am. Chem. Soc. 46 (1924) 1858–1881.
[14] S. Salunke-Gawali, L. Kathawate, V.G. Puranik, J. Mol. Struct. 1022 (2012) 189–196.
[15] Y. Shinde, S. Sproules, L. Kathawate, S. Pal, V.B. Konkimalla, S. Salunke-Gawali, J. Chem. Sci. 126 (2014) 213–225.
[16] D. Chadar, M. Camilles, R. Patil, A. Khan, T. Weyhermüller, S. Salunke-Gawali, J. Mol. Struct. 1086 (2015) 179–189.
[17] O. Pawar, A. Patekar, A. Khan, L. Kathawate, S. Haram, G. Markad, V. Puranik, S. Salunke-Gawali, J. Mol. Struct. 1059 (2014) 68–74.
[18] S. Pal, M. Jadhav, T. Weyhermüller, Y. Patil, M. Nethaji, U. Kasabe, L. Kathawate, V.B. Konkimalla, S. Salunke-Gawali, J. Mol. Struct. 1049 (2013) 355–361.
[19] R. Patil, S. Bhand, V.B. Konkimalla, P. Banerjee, B. Ugale, D. Chadar, S. Kr. Saha, P. Priyadarshi Praharaj, C.M. Nagaraja, D. Chakrovarty, S. Salunke-Gawali, J. Mol. Struct. 1125 (2016) 272–281.
[20] D.D. Perrin, W.L. Armarego, D.R. Perrin, Purification of Laboratory Chemicals, Pergamon Press, London, 1988, p. 260.
[21] D. Chaudhari, S.P. Gejji, D.N. Lande, D. Chakravarty, Sunita Salunke-Gawali, J. Mol. Struct. 1120 (2016) 281–293.
[22] Bruker, APEX2, SAINT, SADABS, Bruker AXS Inc, Madison, Wisconsin, USA, 2007.
[23] G.M. Sheldrick, Acta Cryst. A 64 (2008) 112–122.
[24] L.J. Farrugia, J. Appl. Cryst. 45 (2012) 849–854.
[25] C.F. Macrae, I.J. Bruno, J.A. Chisholm, P.R. Edgington, P. McCabe, E. Pidcock, L. Rodriguez Monge, R. Taylor, J. van de Streek, P.A. Wood, J. Appl. Crystallogr. 41 (2008) 466–470.
[26] A.L. Spek, Acta Cryst. D65 (2009) 148–155.
[27] M. J.Frisch, G. W.Trucks, H. B. Schlegel, G. E. Scuseria, M. A. Robb, J. R. Cheeseman, G. Scalmani, V. Barone, B. Mennucci, G. A. Petersson, et al, Gaussian, Inc., Wallingford CT, 2009.
[28] R. Dennington, T. Keith, J. Milliam, Semichem Inc., Shawnee Mission, KS, 2009.
[29] S. Sarker, L. Nahar, Y. Kumarasamy, Methods 42 (2007) 321–324.
[30] S. Patil, S. Athare, A. Jagtap, K. Kodam, S. Gejji, D. Malkhede, RSC Adv. 6 (2016) 110206–110220.
[31] S. Salunke-Gawali, L. Kathawate, V.G. Puranik, J. Mol. Struct. 1022 (2012) 189–196.
[32] U. Ali Dar, S. Bhand, D.N. Lande, S.S. Rao, Y.P. Patil, S.P. Gejji, M. Nethaji, T. Weyhermüller, S. Salunke-Gawali, Polyhedron 113 (2016) 61–72.
[33] A.V. Todkary, R. Dalvi, S. Salunke-Gawali, J. Linares, J. Marrot, F. Varret, J.V. Yakhmi, M. Bhadbhade, D. Srinivas, S.P. Gejji, S.Y. Rane, Spectrochim. Acta A 63 (2006) 130–138.
[34] L. Kathawate, S. Sproules, O. Pawar, G. Markad, S. Haram, V. Puranik, S. Sunita-Gawali, J. Mol. Struct. 1048 (2013) 223–229.
[35] S. Sunita-Salunke, L. Kathawate, Y. Shinde, V.G. Puranik, J. Mol. Struct. 1010 (2012) 38–45.